An Induction Machine Design with Parameter Optimization for a 120 kW Electric Vehicle

Nan Zhao, *Member, IEEE*, and Nigel Schofield, *Member, IEEE*

***Abstract*—Electric traction machines have been applied to both industrial variable speed applications and electric vehicles. The induction machine (IM) is a potential candidate for traction machines due to the established industrial base. However, most of the existing studies on traction IM design rely on optimization algorithms or iterative calculation programs that subsequently give no clear understanding of the design requirements for field-weakening or extended speed operation. Hence, published procedures to guide IM design for traction applications are somewhat ad hoc to-date. This paper identifies the key IM design parameters required to achieve a traction characteristic within power supply constraints. As an example, a 120 kW electric vehicle traction machine is studied as a benchmark machine and then the proposed design procedure is employed to re-design the machine to improve its extended speed performance. Improvements in terms of efficiency and field-weakening capability are presented. Experimental results from the benchmark machine are used for validation of the subsequent simulation studies reported in this paper. Finally, the identified parameters are shown to be similar with brushless permanent magnet machines. Thus, a generalized machine design philosophy can be concluded.**

***Index Terms*—Induction motors, machine design, traction motor drives, power electronics.**

I. Introduction

The operational characteristics of traction systems, i.e. high torque at low speed and constant power from base speed to high speed, are typical requirements in many electrical drive system applications. The constant power speed ratio (CPSR), or maximum speed to full-load base speed ratio, varies with application, for example, the ratio may be 2:1 for lift machinery [1] and some home appliances [2], 3:1 for computer numeric controlled machine tools [3] and more recently, 2 to 3:1 for electric and hybrid-electric vehicle systems [4].

The induction machine (IM) is a mature technology and a suitable candidate for traction applications. IMs designed for traction applications are supplied via power electronic (PE) converters, rather than being connected direct-on-line (DOL) to a fixed voltage, fixed frequency (FVFF) power grid. DOL connected IMs are currently the main machine technology used in industry with a figure of 80% typically quoted [5]. However, PE driven IMs, in variable torque-speed drive applications, are becoming more popular since they offer a wider rectangular torque-speed characteristic envelope from zero to full-load base speed, improved system dynamics and potential for higher system energy conversion efficiencies. Traction applications also extend the IM torque-speed characteristic further towards a maximum speed by field-weakening [6, 7]. Generally, high torque at low speed and constant power at high speed are the main initial design requirements for traction machines [8, 9]. Therefore, a higher value of CPSR is conducive to the reduction of machine and PE rating [7], which requires a higher maximum torque to nominal torque ratio [10-13]. The authors in [11-13] pointed out that the machine maximum torque can be improved by changing the machine slot geometry and airgap to obtain lower stator and rotor leakage inductance. In addition, the use of variable speed drives yields new design freedoms compared to FVFF driven IMs that can be used in the traction design procedure. Popescu *et al.* [14] introduced flat wire-hairpin-winding to improve the machine maximum starting continuous torque and power. In order to improve IM field weakening performance, Guan *et al.* [15] assessed the influence of machine equivalent circuit parameters and Seo *et al.* [16] investigated the geometry details of IM stator and rotor. However, the aforementioned publications only provide methods to improve some certain aspects of conventional IM performance. Thus, a complete traction machine design procedure needs to be explored.

The design procedures proposed in [17-20] extended the conventional IM design to an iterative design program over the full IM speed range. However, these methods rely on the developed software for simulation iterations and is time consuming. More importantly, there is no clear guidance and solutions for achieving the traction characteristics. The work in [21] presented an IM design procedure for field-weakening operation. It is carried out to evaluate IM parameters to achieve a given field-weakening region of operation and then the machine dimensions are obtained by solving a system of non-linear equations based on the evaluated parameters. However, this design procedure is highly dependent on the machine mathematical model and hence the key IM design parameters cannot be determined.

Most existing literatures paid much attention on optimization procedures to maximize IM performance, hence the induction machine is required to be expressed as mathematical functions for optimization algorithms [22]. For example, optimization algorithms in [23-25] were developed for maximizing the ratio of maximum torque to nominal torque, starting torque and minimizing machine mass and volume respectively. The design strategies proposed in [26, 27] determined the optimum rotor

N. Zhao is with the School of Electrical and Electronic Engineering, University College Dublin, Belfield, Dublin 4, Ireland (e-mail: nan.zhao@ucd.ie).

Nigel Schofield is with the School of Computing and Engineering, University of Huddersfield, Huddersfield, HD1 3DH, UK (e-mail: n.schofield@hud.ac.uk).

slot shape for maximum efficiency. Furthermore, a trade-off among the different constraints in terms of supply voltage, pole number and maximum speed was investigated in [28]. However, a wide multidimensional variable design space is required to optimize the machine for all operating points, which is difficult to implement and extremely time consuming for FEA evaluation. In addition, the machine field-weakening capability is rarely considered by the existing optimization algorithms.

To design a traction machine within the voltage and current constraints imposed by the PE converter, it is necessary to have a clear design procedure with identification of the key machine design parameters. For brushless permanent magnet (PM) machines, the back-EMF coefficient, k_o^{PM}, primarily impacts on the machine maximum torque from zero to base speed. In the field-weakening region, the ratio between k_o^{PM} and the *d*-axis inductance-current product, L_dI_{sd}, becomes the main design factor to ensure constant power range [29, 30]. Similarly, for switch reluctance (SR) machines, extended-speed operation can be achieved by reducing the number of turns per phase from that optimized for maximum torque/Ampere at base speed, with the compromise being a reduction of torque/Ampere below base speed [31], which is effectively the same procedure as for brushless permanent magnet machines, i.e. tuning the k_o^{PM}/L_dI_{sd} ratio. Although the machine traction characteristics have been compared between IM, PM and SR machines [32-34], the key design parameters that determine that ensure extended speed, or field weakening, operation are not discussed.

Thus, this paper identifies the key parameters for IM design such that the design achieves a traction characteristic within PE and supply constraints. The paper then presents an improved IM design procedure that gives a clear guidance to traction machine design. As an example of the design study, a 120 kW peak electric vehicle induction machine is studied as a benchmark design. The 120 kW machine was the prime mover for a range of early all-electric delivery vehicles. While the torque at low speed was sufficient it was found with increasing road experience that the high speed power was not suitable for sub-urban driving. This study uses experimental results from the benchmark machine to validate finite element analysis (FEA) models that are used to confirm the choice of IM parameters suitable to result in an extended speed capacity, and thus the new design procedure. The design procedure is used to re-design the benchmark machine to achieve an improved traction characteristic in terms of field-weakening capability and efficiency. The proposed design procedure helps to clarify and inform designers of the major machine parameters influencing extended speed capability, thus focusing the design philosophy.

II. Traction Machine Design Methodology

For a given PE converter driven traction machine, the machine stator phase current is limited by the PE converter and machine thermal rating. The stator phase current vector angle is chosen to keep the machine operating at maximum torque-per-Ampere (MTPA) until the maximum phase voltage constrained by the DC link voltage is reached at the base speed [35]. If the supply frequency keeps increasing, the machine enters to the field-weakening region. At the beginning of the field-weakening region, the machine can produce more peak output power than rated power because of the increase of power factor [36]. However, with the increase of supply frequency and slip speed, the IM inductive reactance dominates resulting in reduced output power to a point where peak power cannot be realized at higher speeds. The ratio of this speed to the base speed is defined as constant power speed ratio (CPSR) [37] and the motor power rating decreases with the increase of CPSR [9].

To explore the choice of suitable IM parameters it is noteworthy to review the requirements for brushless permanent machines (PMs) designed for operation in the field weakened or extended speed region.

With the implementation of the rotor field orientation, machine rotor excitation field is aligned with the *d*-axis and the open-circuit back-EMF to the q-axis. However, the excitation field of brushless PM and induction machines are provided by PMs and rotor current respectively. PM machines with surface mounted rotor magnets (SPM) have a non-salient rotor structure which is same as per induction machines, hence SPM machine analysis is employed to make a comparison with IM analysis. For SPM machines, if one neglects all the machine loss mechanisms, the maximum electro-magnetic torque is derived as [38]:

$$T_e^{PM} = 3pk_o^{PM}I_{sq} \tag{1}$$

where p is the machine pole-pairs. In this case, since the direct- and quadrature-axis inductances are equal, i.e. $L_d = L_q$, the current excitation angle equals to zero. Hence, the SPM machine maximum torque, from zero to base speed, is determined by q-axis current I_{sq} and back-EMF coefficient k_o^{PM}.

The SPM machine rotor speed is derived as [38]:

$$\omega_r^{PM} = \frac{\left|V_s^{PM}\right|}{p\sqrt{\left(k_o^{PM} + L_dI_{sd}\right)^2 + (L_qI_{sq})^2}} \tag{2}$$

Theoretically, the machine maximum speed is achieved when the current excitation angle equals to 90 degrees:

$$\omega_r^{PM\,(\max)} = \frac{\left|V_s^{PM\,(\max)}\right|}{p\left|k_o^{PM} - L_dI_{sd\,(\max)}\right|} \tag{3}$$

It can be noticed that if the machine back-EMF coefficient, k_o^{PM}, equals the product L_dI_{sd}, the maximum achievable speed is theoretically infinite, which is informative in illustrating design and operational trends.

In the same way, the IM electro-magnetic torque and synchronous speed can be derived by neglecting all of the machine losses [39, 40]:

$$T_e^{IM} = 3p\frac{L_m^2}{L_r}I_{sd}I_{sq} = 3p\frac{L_m^2}{L_r}I_s^2\sin\gamma\cos\gamma \tag{4}$$

$$\omega_e^{IM} = \frac{\left|V_s^{IM}\right|}{p\sqrt{\left(\frac{L_m^2I_s}{L_r} - L_sI_{sq}\right)^2 + (L_sI_{sd})^2}} \tag{5}$$

Note, L_s is the stator inductance and is equal to the induction machine direct- and quadrature-axis inductances, i.e. $L_s = L_{sd} =$

L_{sq}, L_m is the stator-to-rotor mutual inductance, L_r the rotor inductance, and p the number of pole-pairs, as discussed in [39].

In addition, since the IM stator and rotor leakage inductances are much smaller than the magnetizing inductance, the maximum torque and speed equations can be further simplified from (4) and (5), by neglecting the stator and rotor leakage flux, to give equations (6) and (7) respectively:

$$T_e^{IM\,(\max)} = 3pk_o^{IM} I_{sq} = \frac{3pL_m I_s^2}{2} \tag{6}$$

$$\omega_e^{IM\,(\max)} = \frac{\left|V_s^{IM\,(\max)}\right|}{p\left|L_s I_{sd}\right|} \tag{7}$$

where k_o^{IM} is induction machine back-EMF coefficient which equals to $L_m I_{sd}$.

Equations (4) and (6) indicate that, for certain magnitudes of stator current, maximum torque can be achieved by maintaining γ at 45 degrees from zero to base speed. Hence, similar to SPM machines, the induction machine maximum torque, from zero to base speed, is also determined by the q-axis current I_{sq} and induction machine back-EMF coefficient, k_o^{IM}. According to (7), the minimum value of d-axis inductance-current product, $L_s I_{sd}$, determines the maximum achievable speed. However, to ensure constant power operation, I_{sd} has to be kept above a certain value. Thus, L_s is the only variable that may be adjusted to extend the constant power region. On the other hand, the reduction of L_s results in the decrease of k_o^{IM}, and hence the rotor design will have to be adjusted to compensate. Therefore, under the assumption of negligible loss, induction machines and brushless PM machines have similar key design parameters, which leads to a similar, and importantly, a more informed design procedure.

III. IM Design Procedure for Traction Applications

A. IM design at base speed

According to Equation (4), the induction machine torque is a function of γ for certain magnitudes of stator current and it can be maximized when γ is optimized. Corresponding to the machine constant torque region, the induction machine MTPA trajectory is ideally achieved by maintaining γ at 45 degrees from zero to base speed, although the actual MTPA trajectory deviates from the ideal trajectory due to saturation effects, as illustrated in Fig. 1 (path A-B). The current-limit circle in Fig. 1 is determined by the maximum stator phase current. The voltage-limit ellipses are determined by the phase voltage corresponding to different supply frequencies. Therefore, from the machine operation point of view, the machine base speed point should be set at point B in Fig. 1.

From the machine design point of view, the maximum torque at base speed is directly determined by the machine magnetizing inductance:

$$L_m = 2\mu_0 \frac{m}{p}\left(\frac{N_1 K_{dp1}}{\pi}\right)^2 l_{ef}\frac{\tau}{\delta_{ef}} \tag{8}$$

where μ_0, m, p, N_1, K_{dp1}, l_{ef}, τ and δ_{ef} represent the permeability of vacuum, phase number, pole-pair, number of stator winding turns, winding factor, effective core length, pole-pitch and effective airgap length respectively. For fixed machine dimension, N_1 and δ_{ef} are the key variables to adjust the magnetizing inductance.

In addition, rotor design impacts the machine maximum torque. Shallow rotor slots can be used for traction machine design, which reduces the leakage flux and hence increase the magnetizing flux [41, 42]. Further, the reduction of leakage inductance will improve the machine field weakening capability.

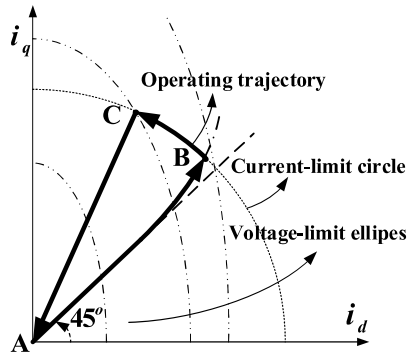

Fig. 1. IM operating trajectory.

B. IM design at maximum speed

With increased supply frequency, although the stator current is still maintained at maximum, the voltage provided by the PE converter is not large enough to maintain the MTPA trajectory. In this case, the d-axis component of stator current deceases with an increase of stator phase current vector angle, resulting in the machine field-weakening region, as shown in Fig. 1 (path B-C). In this region, the stator phase current vector angle is between 45 to 90 degrees and the machine output power is reduced with increase of the value of γ, as shown below:

$$P = \frac{L_m^{\,2} i_s^{\,2}}{L_r}\left(\omega \sin 2\gamma - \frac{pR_r}{L_r}\sin^2\gamma\right) \tag{9}$$

Therefore, to achieve a high value of CPSR, the maximum speed of the constant power region is another design target. According to Equation (7), the machine speed is maximized by reducing stator inductance L_s which is the sum of magnetizing inductance L_m and stator leakage inductance L_{sl}. Hence, from the machine design point of view, the machine maximum speed is mainly determined by the number of stator series turns per phase. At the same time, the stator phase current vector angle γ is also reduced at high speeds, which extends the machine constant power region.

C. IM design procedure for traction applications

Although IM design for traction applications is different from that of the conventional DOL IM, the classical design method can be used to initialize the traction machine design procedure. Classical IM design typically proceeds from the application of classical sizing equations. According to the torque and power requirements at the rated operating point, the machine electric and magnetic loadings are determined by previous experience, given the method of cooling and the lamination material and hence the machine dimension, slot geometry and stator winding are chosen using established

empirical sizing formula. Then, the flux densities of the machine slots, yokes and air gap are calculated by machine magnetic circuit analysis. Discriminant analysis is applied to check the flux densities of different parts of the machine stator and rotor laminations.

However, conventional DOL IMs are designed to satisfy high start-up torque and overload capabilities, the consequence of which leads to the stator phase current vector angle γ differing from 45 degrees. For variable-speed IMs, the magnitude and frequency of the supply voltage can be adjusted to manage the starting requirements, hence, more attention can be paid to the requirements of MTPA and field weakening operations. The value of γ at base speed can be effectively decreased to 45 degrees by reducing machine magnetizing reactance. Therefore, the machine can be designed with maximum torque per Ampere-turns by reducing the number of winding turns. Note, maximum torque per Ampere-turns is different from MTPA. Due to the maximum current limitation imposed by the power electronics, the reduction of stator winding turns leads to a deceased machine electrical loading, reducing the maximum torque in the constant torque region. On the other hand, it decreases the value of L_s and hence γ at high speed, which extends the machine constant power region. Furthermore, the machine conduction loss is significantly decreased with the reduction of the number of winding turns. This trade-off is typical of other machine technologies, i.e. PM [29] and SR machines [31].

The decrease of torque due to reduced stator turns can be compensated by the rotor re-design. As discussed previously, PE converters control current and frequency. Hence, large rotor resistance for starting at line frequency is no longer a requirement. Therefore, conventional deep and narrow rotor slots can be replaced by shallow and wide ones. In this way, the geometric centres of rotor bars will be closer to the rotor outer surface to increase the torque production. Additionally, rotor leakage inductance will be reduced to benefit the high speed performance.

After the analytic study the machine performance is subsequently confirmed via detailed finite-element analysis that accounts for magnetic saturation. Here the design is further optimized for phase current, drive requirements and machine efficiencies.

In summary, the traditional philosophy for traction IM design has been to (i) design a machine capable of peak torque and power at the base speed operating point, and then (ii) to analyze the design to test suitability for extended speed. Invariably the first design iteration will have poor extended speed capability because it is focused by maximizing torque per Ampere. Hence, the first design has to be iterated until a suitable solution is realized. While the outcome is arguably a solution, the designer does not have a fundamental appreciation of what drives the design solution. However, the proposed design procedure discussed here clearly informs the designer of the major design parameters influencing extended speed capability, thus focusing the design choices, this is a contribution of the paper. The conventional design procedure (dashed-box) is thus modified to capture the ideas discussed here in a new Traction IM Design Procedure (solid-box), as illustrated in Fig. 2. The key IM electro-magnetic parameters are now identified and thus focus the traction machine design. The design process is still iterative in terms of the thermal, loss and mechanical considerations.

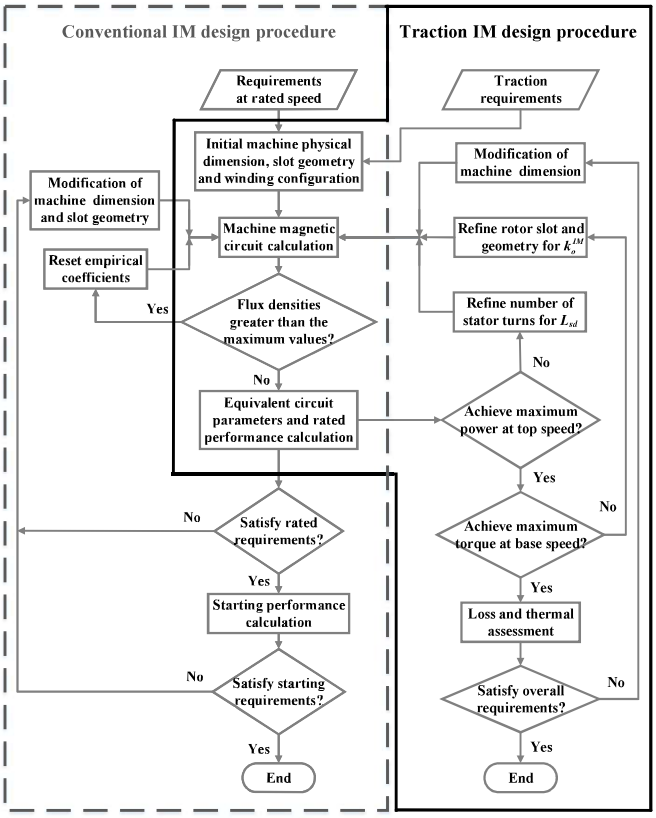

Fig. 2. IM design procedure for conventional and traction application.

IV. Redesign of an Example Traction IM

A. Benchmark traction induction machine

An example traction induction machine, the P120, used for the 7.5 tonne Smith Newton electric vehicle, is studied as a reference benchmark machine, as shown in Fig. 3. This machine is designed to have 120 kW peak power at 1800 RPM and top speed of 7200 RPM. The benchmark machine (Motor 1) design parameters are detailed in Table I, while the machine dimension is shown in Fig. 4. This machine is modeled by finite element analysis (FEA) software and the FEA model validated by machine test data provide by Smith EV, USA, as illustrated in Fig. 5 (for the 7-turn design). Keeping the FEA torque and power consistent with the measured torque and power, the phase current is calculated and compared with the measured phase current. The FEA and measured data show good agreement, hence the FEA analysis tool is used for further redesign analysis. Here, two points on the torque-speed characteristic are considered as key for design; (i) Point 1 is 640 Nm at 1800 RPM, which is the maximum speed point at which maximum torque can be delivered. This point determines the machine and traction power electronic inverter maximum current rating. (ii) Key Point 2 refers to the maximum torque at top speed (7200 RPM). However, due to the machine design and DC-link voltage limit, the original machine cannot is not capable to achieve 120 kW over the desired extended speed range, as shown in Fig. 5.

Fig. 3. Smith Newton electric vehicle and traction machine.

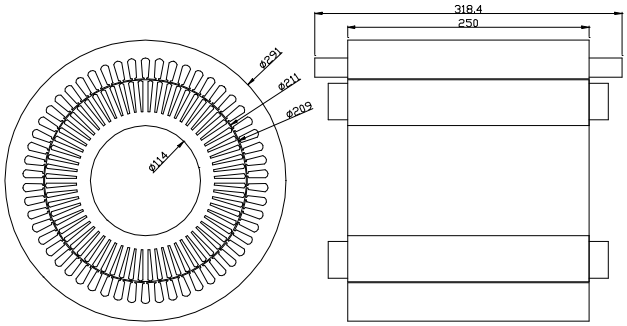

Fig. 4. Main dimension of P120 traction IM.

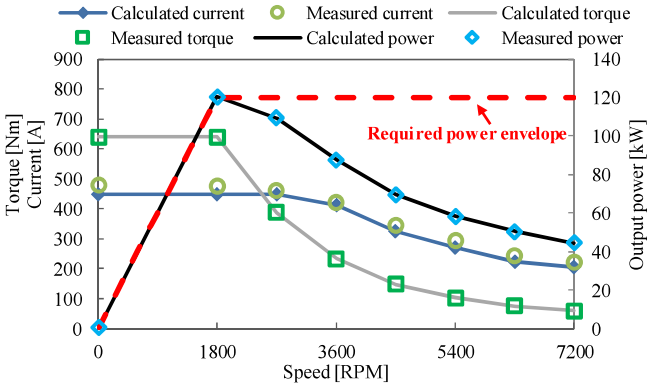

Fig. 5. Experimental torque, power and phase current characteristics of the benchmark machine.

B. Traction induction machine design study

As discussed above, machine constant power region can be extended by reducing the number of stator series turns per phase. Hence, by maintaining the dimensions and lamination geometry of the benchmark IM, the machine torque and power performance with a variable number of stator winding turns is investigated, as illustrated in Fig. 6. It can be noticed that with reducing turns, from 7 to 4, the machine high speed performance is improved, in Fig. 6 (a). However, with fixed phase current, reduction of winding turns reduces electrical loading and hence the maximum torque in the constant torque region is reduced, as illustrated in Fig. 6 (b). This is the design trade-off. Moreover, according to Equation (7), the value of *d*-axis inductance-current product, L_sI_{sd}, determines the machine maximum speed of constant power region. When the machine operates above the maximum speed of constant power region, it is driven along the maximum torque per volt (MTPV) trajectory, as illustrated in Fig. 1 (path C-A).

Therefore, the stator current of benchmark machine (7 turns) reduces significantly with the increase of speed, as illustrated in Fig. 6 (c). Since the constant power region is extended with the reduction of winding turns, the machine enters to the MTPV region at higher speed and hence the phase current starts to drop at higher speed. The decrease of torque due to reduced stator turns can be compensated by the rotor redesign. As discussed previously, conventional deep and narrow rotor slots can be replaced by shallow and wide ones, as shown in Fig. 7. In this way, magnetizing inductance is increased due to the reduction of leakage flux. Note, since the stator phase current vector angle is robust to the rotor resistance and reactance, the machine MTPA will not be impacted.

With the same constraints of the benchmark IM (Motor 1), a new IM (Motor 2) with the same rotor bar material (aluminium) is designed by utilizing the proposed procedure. The machine rotor slot geometry is illustrated in Fig. 7 (b) and design parameters are detailed in Table I. Motor 2 has the same stator winding scheme with Motor 1, but it has lower number of turns. Keeping the same stator slot area, the lower number of turns allows an increase in the conductor diameter to further reduce the resistance.

In addition, compared to Motor 1, shallow and wide slots are applied to Motor 2. Hence, the number of rotor bars is reduced to be 58, which keeps the torque ripple within the constraint. Although the reduction of slot area leads to higher real rotor resistance, the equivalent rotor resistance may be reduced due to the decrease of the number of stator series turns per phase.

To investigate the influence of a more conductive rotor bar on the traction characteristic, aluminium bars are replaced with copper. Thus, maintaining the same stator design of Motor 2, the machine rotor is redesigned with die-cast copper bars (Motor 3). However, die-cast copper bars will introduce design issues in terms of manufacture and mechanical stress. Motor 3 is therefore used to investigate the electromagnetic performance influenced by more conductive materials without considering the mechanical stress issue. The rotor slot area is further reduced as illustrated in Fig. 7 (c) and design parameters are detailed in Table I.

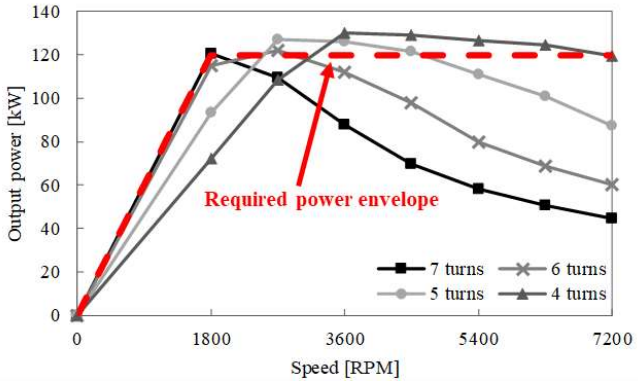

(a) Output power versus speed.

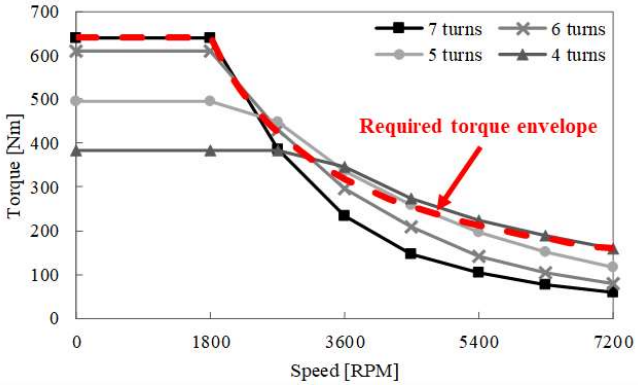

(b) Torque versus speed.

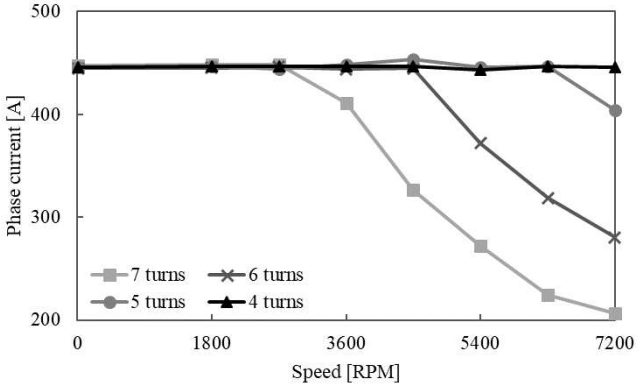

(c) Phase current versus speed.

Fig. 6. Machine performance as a function of stator winding turns.

hence achieves a 1.7% higher efficiency at 1800 RPM. Reducing the turns increases the flux for the same applied voltage, hence the machine flux density is slightly larger compared to the benchmark machine, as shown in Fig. 9 (a) and (b), which slightly increase the iron loss. Fig. 10 (a) compares the airgap flux density of the two machines at 1800 RPM. More importantly, due the reduction of stator inductance L_s, higher current is achieved in the extended speed region, hence, Motor 2 significantly increase the power output by 48.6% at 7200 RPM. Due to limited DC-link voltage, both Motor 1 and 2 operate in field-weakening region, as shown in Fig. 9 (c) and (d). However, Motor 2 has higher airgap flux density than Motor 1, as illustrated in Fig. 10 (b), which leads to higher output power.

Table I. Machine design details.

	Motor 1	Motor 2	Motor 3
Stator outer diameter (mm)	291		
Stator inner diameter (mm)	211		
Rotor outer diameter (mm)	209		
Rotor inner diameter (mm)	114	135	145
Machine active axial length (mm)	250		
Number of poles	6		
Number of stator slots	54		
Number of rotor slots	64	58	64
Number of turns per phase	7	6	6
Stator winding	double-layer distributed		
Rotor bar material	aluminium		copper
Stator copper mass (kg)	10.88	10.88	10.88
Stator iron mass (kg)	43.83	43.83	43.83
Rotor conductor mass (kg)	6.95	4.34	10.25
Rotor iron mass (kg)	29.66	29.14	27.40
Total mass (kg)	91.32	88.19	92.36

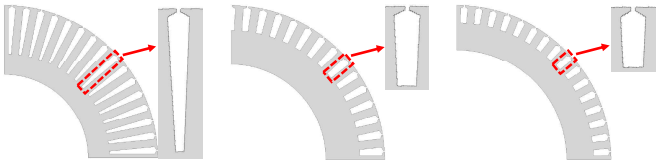

(a) Motor 1. (b) Motor 2 (c) Motor3

Fig. 7. Comparison of IM rotor slots.

C. *Machine performance and analysis*

Fig. 8 illustrates the machine performance results within the same supply voltage and current constraints. Tables II and III compare the results for Motors 1, 2 and 3 at 1800 RPM and 7200 RPM respectively. Compared to Motor 1, Motor 2 maintains the same maximum torque at corner speed. Note, since the airgaps, associated bearings, mechanics etc. of the original and proposed machines are the same, the mechanical losses will be similar, hence have not been included here clarity of the electro-magnetic discussion.

Due to the reduction of stator resistance and equivalent rotor resistance, it contributes a 22% reduction in Joule loss and

For Motor 3, the rotor slot area is further reduced by using copper in Fig. 7 (c). However, it has almost same value of L_s with Motor 2. Compared to Motor 2, the torque-speed characteristics of Motor 3 is slightly improved, as illustrated in Fig. 8 (b). The efficiency of Motor 3 is higher than Motor 2 at 1800 RPM due to the more conductive rotor bar, but it is lower at 7200 RPM due to the higher phase current. Therefore, using more conductive materials will not significantly improve the machine torque-speed characteristics. From which it is concluded that the IM key design parameters of k_o^{IM} and L_s highly impact on the achievable traction characteristic within PE and supply constraints. After the corner speed of 1800 RPM,

the machine operation is limited by the supply voltage, which requires the current vector to rotate towards the q-axis until the maximum torque per voltage (MTPV) is achieved [43, 44]. Therefore, in the speed range of 1800 RPM to 3600 RPM, the machine power factor initially increases (1800 RPM to 2700RPM) and then reduces (from 2700 RPM to 3600 RPM), as shown in Fig. 8 (d). To keep constant power, the supply current is reducing in the speed range of 1800 RPM to 2700 RPM and then increases again, as shown in Fig. 8 (c). Furthermore, the leakage inductance of the three motors is calculated and shown in Fig. 8 (f), which takes the load-dependent local saturation into account. Due the reduced stator winding turns and the redesigned rotor slots, Motor 2 and 3 achieve lower leakage inductance than Motor 1, which improves the machine field weakening performance. Note that for Motor 3, the design change to realise high speed operation results in a small compromise in terms of torque ripple (increase of approx. 3%).

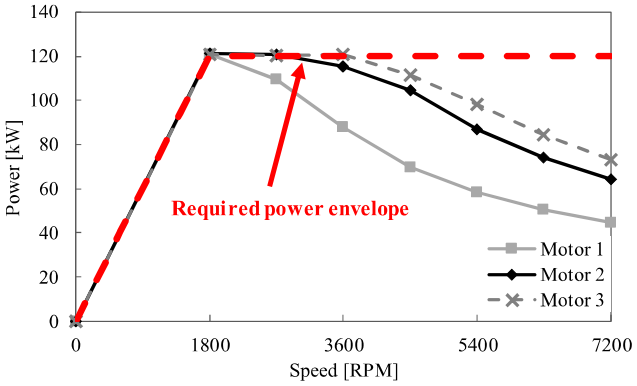

(a) Output power versus speed characteristics.

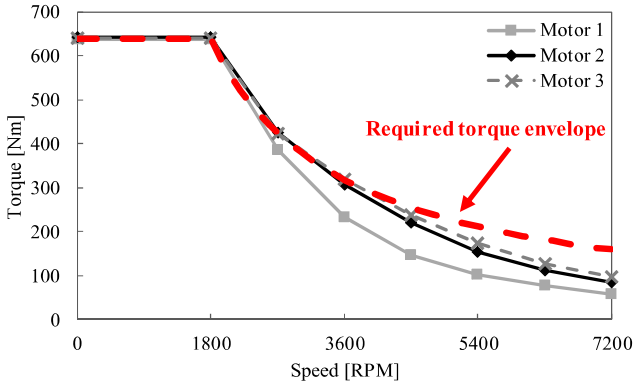

(b) Torque versus speed characteristics.

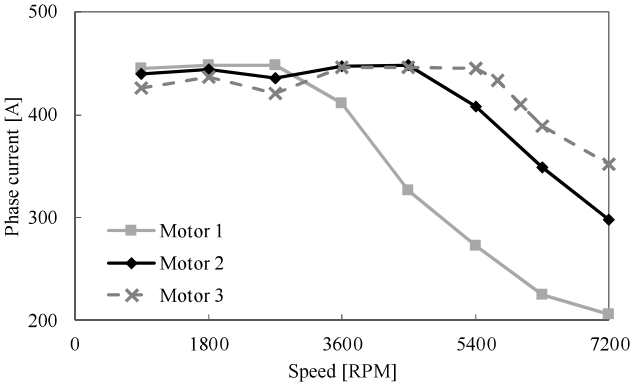

(c) Phase current versus speed.

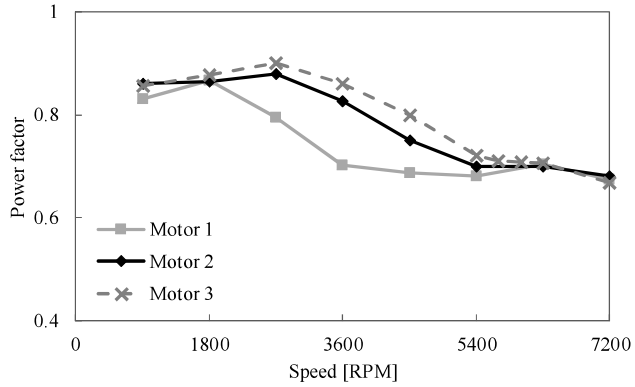

(d) Power factor versus speed.

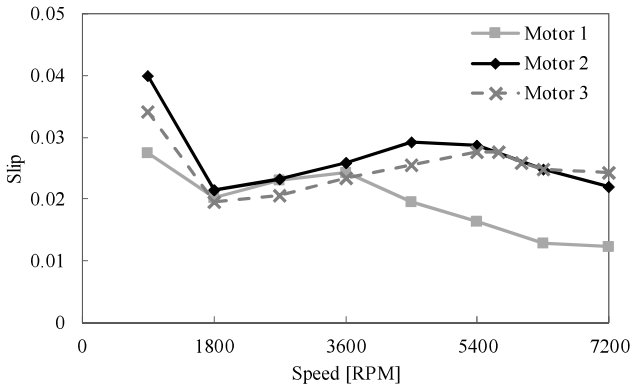

(e) Slip versus speed.

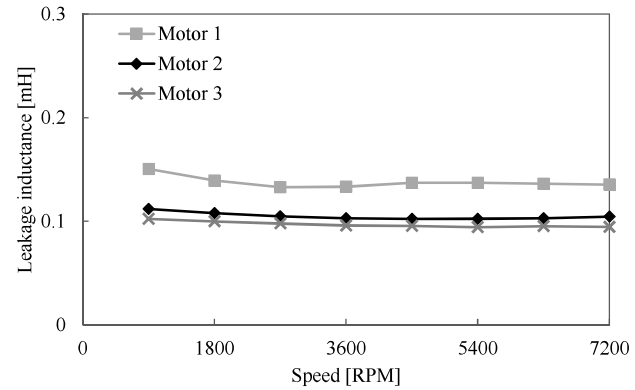

(f) Leakage inductance versus speed.

Fig. 8. Performance comparison of the machine designs.

Table II. Comparison of Machine Performance at 1800 RPM.

	Motor 1	Motor 2	Motor 3
Power (kW)	120.52	121.01	120.93
Torque (Nm)	639.38	641.96	641.56
L_d (mH)	2.26	1.51	1.53
Torque ripple (%)	2.16	2.85	2.43
Iphase_rms (A)	448.34	444.09	436.09
Iron loss (W)	296.42	358.30	351.91
Joule loss (W)	11242.09	8821.62	8567.84
Total loss	11597.45	9227.86	8978.69
Efficiency (%)	91.22	92.91	93.09

Table III. Comparison of Machine Performance at 7200 RPM.

	Motor 1	Motor 2	Motor 3
Power (kW)	44.45	64.17	73.11
Torque (Nm)	58.95	85.11	96.96
L_d (mH)	2.42	1.80	1.80
Torque ripple (%)	5.77	5.23	8.24
Iphase_rms (A)	206.13	297.97	351.46
Iron loss (W)	242.90	391.16	410.83
Joule loss (W)	2535.11	4301.59	6076.91
Total loss	3721.01	5635.74	7430.73
Efficiency (%)	92.28	91.93	90.77

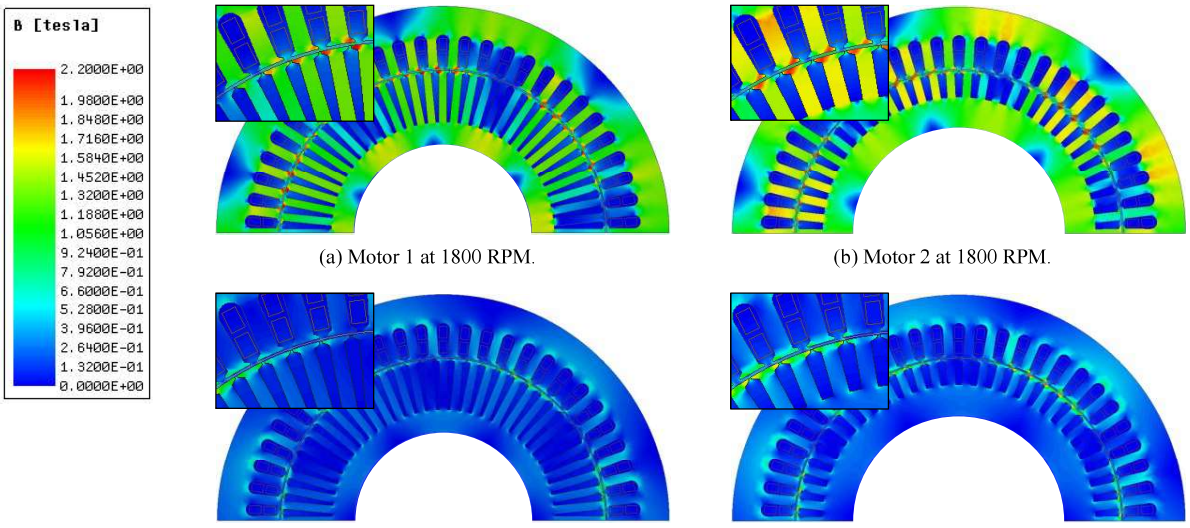

(a) Motor 1 at 1800 RPM. (b) Motor 2 at 1800 RPM.

(c) Motor 1 at 7200 RPM. (d) Motor 2 at 7200 RPM.

Fig. 9. Flux distributions of Motor 1 and 2.

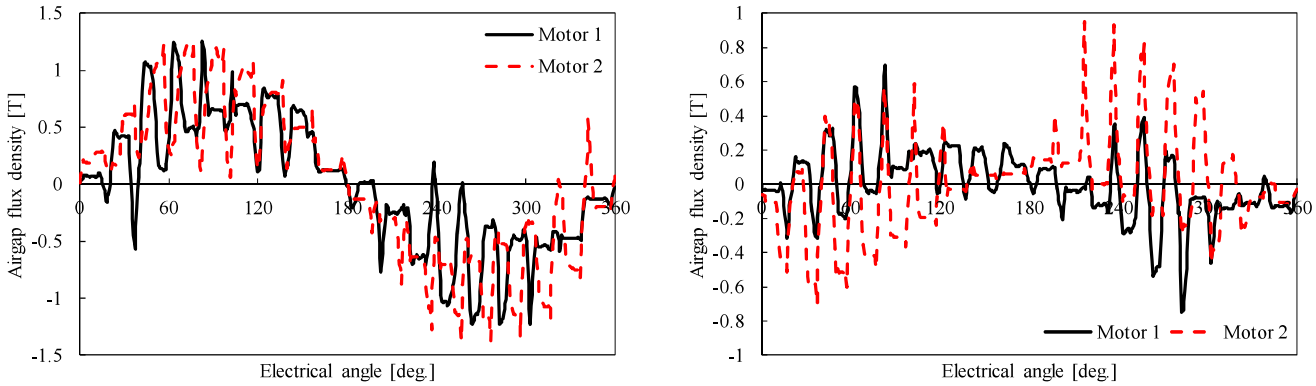

(a) 1800 RPM (b) 7200 RPM

Fig. 10. Airgap flux density of Motor 1 and 2.

D. Final traction induction machine design

The rotor of Motor 2, with aluminium rotor bars, keeps the comparable cost and manufacturing difficulty with the benchmark machine. Therefore, maintaining the same rotor design of Motor 2, the number of winding turns is further reduced to 4 (referred to as Motor 4). With lower value of L_s, Motor 4 achieves a constant power region from 1800 RPM to 7200 RPM. Compared to the benchmark machine, Motor 4 requires a higher phase current of 654.53 A to satisfy the target maximum torque at 1800 RPM, as illustrated in Fig. 11 and Table IV. Although the maximum current of Motor 4 is higher than the benchmark machine, the Joule loss is significantly reduced and hence efficiency improved to achieve the maximum torque.

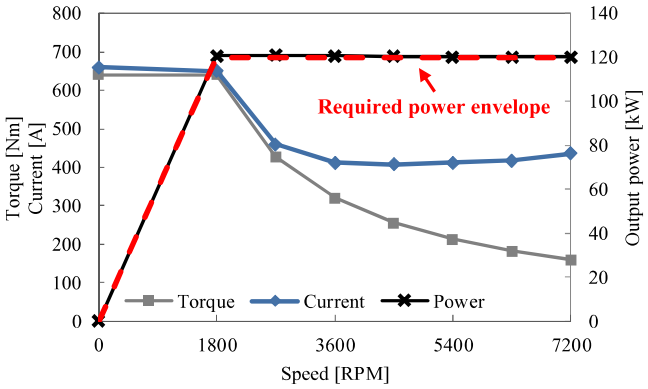

Fig. 11. Performance results for Motor 4.

Table IV. Performance of Motor 4.

	1800 RPM	7200 RPM
Power (kW)	120.98	120.88
Torque (Nm)	641.82	160.32
L_d (mH)	0.65	0.81
Torque ripple (%)	1.78	3.24
Iphase_rms (A)	654.53	438.16
Iron loss (W)	329.71	554.07
Joule loss (W)	7890.69	4169.19
Total loss	8279.34	5666.25
Efficiency (%)	93.60	95.52

V. Conclusions

Traction machines, supplied via PE converters, have to be designed for the complete power-speed characteristic rather than starting and rated operating points as would generally be the case for FVFF IMs. Therefore, the machine design procedures are different. According to existing published works on variable speed IM design, most of the machine design relies on optimization algorithms or iterative calculation programs and the key parameters for machine design are thus not clearly identified. This paper identifies the key design parameters influencing the realisation of a traction torque-speed characteristic. These are the back-EMF constant, k_o^{IM}, and the *d*-axis inductance-current product, L_sI_{sd}. Hence, the paper proposes a traction induction machine design procedure that generalizes brushless permanent magnet (PM) machine design procedure to that of IM design when considering designs suitable for extended speed or field weakening operation. At base speed the back-EMF constant, k_o^{IM}, is the dominant parameter. The maximum torque can be achieved by maintaining the stator phase current vector angle, γ, at 45 degrees from zero to base speed. In the constant power region, the minimum value of *d*-axis inductance-current product, L_sI_{sd}, determines the maximum achievable speed. Therefore, the IM extended-speed operation can be achieved by reducing L_s (by reducing the number of turns per phase).

In addition, wide, shallow and open slots are used for traction machine design, which reduces leakage inductance and moves geometric centers of the rotor bars closer to the rotor outer surface to increase torque production.

The design concept is similar to that of PM machine design, where the back-EMF coefficient, k_o^{PM}, is adjusted and the d-axis inductance–phase current product, L_dI_s, increased to improve the extended field weakening region.

The proposed design procedure is applicable across different ratings. As an example, a 120 kW induction machine is studied as a benchmark machine is subsequently redesigned using the proposed design procedure to illustrate the improvement in performance capability and improvements in terms of efficiency, power factor and field weakening capability.

VI. Acknowledgments

The authors thank Prof. S. Williamson for his valued comments and Mr. Jan Elkjaer of Smith EV, USA for vehicle test data and graphics and P120 induction machine data.

References

[1] Zhao, N., Schofield, N., Niu, W., *et al.*: 'Hybrid power-train for port crane energy recovery', Proc. IEEE Transportation Electrification Conf. Expo. Asia-Pacific, Beijing, China, Sept. 2014, pp. 1–6.

[2] Kokalj, D. G.: 'Variable frequency drives for commercial laundry machines', IEEE Industry Applications Magazine, 1997, **3**, (3), pp. 27-30.

[3] Avram, O. I., Xirouchakis, P.: 'Evaluating the use phase energy requirements of a machine tool system', Journal of Cleaner Production, 2011, **19**, (6-7), pp. 699-711.

[4] M. Olszewski: 'Evaluation of the 2010 Toyota Prius hybrid synergy drive system', Oak Ridge Nat. Lab., Oak Ridge, ORNL/TM-2010/253, Mar. 2011.

[5] D. Zorbas, *Electric Machines: principles, applications, and control schematics*, Stamford, CT, USA: Cengage Learning, 2nd edn. (2014).

[6] Ehsani, M., Gao, Y., Gay, S.: 'Characterization of electric motor drives for traction applications', Proc. IEEE Industrial Electronics Society the 29th Annual Conf., Roanoke, USA, Nov. 2003, pp. 891-895.

[7] Ehsani, M., Rahman, K. M., Toliyat, H. A.: 'Propulsion system design of electric and hybrid vehicles', IEEE Transactions on Industrial Electronics, 1997, **44**, (1), pp. 19-27.

[8] Lindh, P., Montonen, J., Tehrani, M. G., *et al.*: 'Design process of a traction motor for a hybrid bus application', Proc. Electric Power Quality and Supply Reliability Conf., Rakvere, Estonia, Jun. 2014, pp. 255-258.

[9] Gao, Y., Ehsani, M.: 'Parametric design of the traction motor and energy storage for series hybrid off-road and military vehicles', IEEE Transactions on Power Electronics, 2006, **21**, (3), pp. 749-755.

[10] Oldenkamp, J. L., Peak, S. C.: 'Selection and design of an inverter-driven induction motor for a traction drive system', IEEE Transactions on Industry Applications, 1985, **IA-21**, (1), pp. 259-265.

[11] Magill, M. P., Krein, P. T.: 'Examination of design strategies for inverter-driven induction machines', Proc. Power and Energy Conf. at Illinois, Champaign, USA, Feb. 2012, pp. 1-6.

[12] De Buck, F. G. G.: 'Design adaptation of inverter-supplied induction motors', IEE Journal Electric Power Applications, 1978, **1**, (2), pp. 54-60.

[13] Cui, S., Bai, Y., Song, L.: 'Rotor slots design of induction machine for hybrid electric vehicle drives', Proc. IEEE Conf. Vehicle Power and Propulsion, Windsor, United Kingdom, Sept. 2006, pp. 1-3.

[14] Popescu, M., Goss J., Staton, D., *et al.*: 'Electrical vehicles—practical solutions for power traction motor systems', IEEE Transactions on Industry Applications, 2018, **54**, (3), pp. 2751-2762.

[15] Guan Y., Zhu Z., Afinowi, I., *et al.*: 'Influence of machine design parameters on flux-weakening performance of induction machine for electrical vehicle application', IET Electrical Systems in Transportation, 2015, **5**, (1), pp. 43-52.

[16] Seo, S., Park, G., Kim Y., *et al.*: 'Design method on induction motor of electric vehicle for maintaining torque performance at field weakening region', Proc. IEEE 20th International Conference on Electrical Machines and Systems, Sydney, Australia, Aug. 2017, pp. 1–5.

[17] Murthy, S. S., Singh, B., Bhuvaneswari, G., *et al.*: 'Design of squirrel cage induction motors for traction applications', Proc. IEEE Conf. Power Electronics, Drives and Energy Systems, New Delhi, India, Dec. 2006, pp. 1-7.

[18] Harson, A., Mellor, P. H., Howe, D.: 'Design considerations for induction machines for electric vehicle drives', Proc. IET Conf. Electrical Machines and Drives, Durham, United Kingdom, Sept. 1995, pp. 16-20.
[19] Liu, H., Zhang, Y., Zheng, Q., *et al.*: 'Design and simulation of an inverter-fed induction motor for electric vehicles', Proc. IEEE Conf. Vehicle Power and Propulsion, Arlington, USA, Sept. 2007, pp. 112–115.
[20] Duan, S., Zhou, L.: 'Influence of parameters on field weakening performance of induction motor', Proc. Int. Conf. Electrical machines and systems, Beijing, China, Aug. 2011, pp. 1–5.
[21] Bianchi, N., Bolognani, S.: 'Design procedure of a vector controlled induction motor for flux-weakening operations', Proc. Industry Applications Conf. Thirty-Second IAS Annual Meeting, New Orleans, USA, Oct. 1997, pp. 104–111.
[22] Agamloh, E. B., Cavagnino, A.: 'High efficiency design of induction machines for industrial applications', Proc. IEEE Workshop on Electrical Machines Design Control and Diagnosis, Paris, France, Mar. 2013, pp. 33-46.
[23] Hecker, Q., Ccoa, J. A. B., Meyer, W., *et al.*: 'Automated design of squirrel-cage induction machines by predefined torque-speed-characteristic', Proc. Int. IEEE Conf. Electric Machines and Drives, Chicago, USA, May 2013, pp. 1160-1165.
[24] Lee, J. H., Ramamurthy, S. S., Yun, T. W.: 'Optimum design for premium 250 kW efficiency of traction induction motor using response surface methodology & FEM', Proc. Int. IEEE Conf. Electrical Machines and Systems, Incheon, South Korea, Oct. 2010, pp. 1844-1847.
[25] Hall, E., Lee, B. D., Balda, J. C.: 'Optimum speed ratio of induction motor drives for electrical vehicle propulsion', Proc. IEEE Applied Power Electronics Conf., Anaheim, USA, Mar. 2001, pp. 371-377.
[26] Williamson, S., McClay, C. I.: 'Optimization of the geometry of closed rotor slots for cage induction motors', IEEE Transactions on Industry Applications, 1996, **32**, (3), pp. 560-568.
[27] Amrhein, M., Krein, P. T.: 'Rotor designs for small inverter-dedicated induction machines', Proc. Int. IEEE Conf. Electric Machines and Drives, Madison, USA, Jun. 2003, pp. 1279-1285.
[28] Zhang, Z., Profumo, F., Tenconi, A.: 'Improved design for electric vehicle induction motors using an optimization procedure', Proc. IEE Electric Power Applications, 1996, **143**, (6), pp. 410-416.
[29] Zhao, N., Yang, R., Schofield, N., *et al.*: 'An investigation of DC-link voltage and temperature variations on EV traction system design', IEEE Transactions on Industry Applications, 2017, **53**, (4), pp. 3707-3718.
[30] Zhao, N., Schofield, N.: 'Field-weakening capability of interior permanent magnet machines with salient pole shoe rotors', IEEE Transactions on Magnetics, 2017, **53**, (11), pp. 1-7.
[31] Schofield, N., Long, S. A., Howe, D., *et al.*: 'Design of a Switched Reluctance Machine for Extended Speed Operation', IEEE Transactions on Industry Applications, 2009, **45**, (1), pp. 116 – 122.
[32] Dorrell, D., Knight, A., Evans, L., *et al.*: 'Analysis and design techniques applied to hybrid vehicle drive machines—assessment of alternative IPM and induction motor topologies', IEEE Transactions on Industrial Electronics, 2012, **59**, (10), pp. 3690-3699.
[33] Guan, Y., Zhu, Z. Q., Afinowi, I. A. A., *et al.*: 'Comparison between induction machine and interior permanent magnet machine for electric vehicle application', Proc. IEEE 17th International Conference on Electrical Machines and Systems, Hangzhou, China, Oct. 2014, pp. 144–150.
[34] Yang, Z., Shang, F., Brown, I., *et al.*: 'Comparative study of interior permanent magnet, induction, and switched reluctance motor drives for EV and HEV applications', IEEE Transactions on Transportation Electrification, 2015, **1**, (3), pp. 245-254.
[35] Alberti, L., Bianchi, N., Bolognani, S.: 'Variable-speed induction machine performance computed using finite-element', IEEE Transactions on Industry Applications, 2005, **47**, (2), pp. 789-797.
[36] Puranen, J.: 'Induction motor versus permanent magnet synchronous motor in motion control applications: a comparative study', PhD thesis, Lappeenranta University of Technology, 2006.
[37] Soong, W. L., Miller, T. J. E.: 'Field-weakening performance of brushless synchronous AC motor drives', Proc. IEE Electric Power Applications, 1994, **141**, (6), pp. 331-340.
[38] Schiferl, R.F., Lipo, T. A.: 'Power capability of salient pole permanent magnet synchronous motors in variable speed drive applications', IEEE Transactions on Industry Applications, 1990, **26**, (1), pp. 115-123.
[39] P. Vas. Vector Control of AC Machines, Oxford, U.K.: Clarendon Press, (1990).
[40] Zhao, N., Schofield, N.: 'An improved induction machine design procedure for electric vehicle traction', Proc. IET International Conference on Power Electronics, Machines and Drives, Glasgow, UK, Apr. 2016, pp.1-6.
[41] Zhao, Z. M., Meng, S., Chan, C. C., *et al.*: 'A novel induction machine design suitable for inverter-driven variable speed systems', IEEE Transactions on Energy Conversion, 2000, **15**, (4), pp. 413-420.
[42] Wang, T., Zheng, P., Zhang, Q., *et al.*: 'Design characteristics of the induction motor used for hybrid electric vehicle', IEEE Transactions on Magnetics, 2005, **41**, (1), pp. 505-508.
[43] G. Pellegrino, A. Vagati, B. Boazzo, and P. Guglielmi, "Comparison of induction and PM synchronous motor drives for EV application including design examples," IEEE Trans. Ind. Appl., vol. 48, no. 6, pp. 2322–2332, Nov./Dec. 2012.
[44] Jussi Puranen, "Induction motor versus permanent magnet synchronous motor in motion control applications: a comparative study," Ph.D. thesis, Lappeenranta University of Technology, 2006.

Nan Zhao (S'15-M'17) received the B.Eng. degree in Electrical Engineering from Taiyuan University of Technology, China, in 2012; the M.Sc. degree in Electrical Engineering from the University of Manchester, UK, in 2013; the Ph.D. degree in Electrical Engineering from McMaster University, Canada, in 2017. He was appointed as a Sessional Lecturer (2017-18) in the Department of Electrical and Computer Engineering, McMaster University, Ontario, Canada. In 2018, Dr. Zhao joined the School of Electrical and Electronic Engineering, University College Dublin, Ireland, as an Assistant Professor. His main research is in the field of electric machines, energy storage systems and related power electronics for transportation electrification and renewable energy systems.

Nigel Schofield (M'06) received the B.Eng. (Hons.) in Electrical Power Engineering, and Ph.D. in electric machine design from the University of Sheffield, UK, in 1990 and 1997, respectively. Dr. Schofield was a Senior Experimental Officer (1993-95), post-doctoral researcher (1997-2001) and Lecturer at the University of Sheffield (2001-04). He was a Design Engineer in industry (1995-97). He was a Lecturer in the School of Electrical and Electronic Engineering, at the University of Manchester, UK, (2004-09) and Senior Lecturer (2009-12). He was a Full Professor with Tenure in the ECE Department, at McMaster University, Ontario, Canada, (2013-17) before joining the University of Huddersfield as Professor of Electrical Engineering, School of Computing and Engineering, in May 2017. Prof. Schofield is a member of the Institution of Engineering and Technology, U.K., and a Chartered Engineer in the U.K.